

Theoretical study of the light-induced conical intersection in the photodissociation of molecule OH

Jinqian Liu(刘金倩), Jialong Li(李嘉隆), Dongdong Zhang(张栋栋), and Dajun Ding(丁大军)
Citation: Chin. Phys. B, 2025, 34 (**10**): 103101. DOI: 10.1088/1674-1056/addcbb
http://cpb.iphy.ac.cn; http://iopscience.iop.org/cpb

What follows is a list of articles you may be interested in

Formation of nanobubbles generated by hydrate decomposition: A molecular dynamics study

Zilin Wang(王梓霖), Liang Yang(杨亮), Changsheng Liu(刘长生), and Shiwei Lin(林仕伟)
Chin. Phys. B, 2023, 32 (**2**): 023101. DOI: 10.1088/1674-1056/ac786a

Effect of conical intersection of benzene on non-adiabatic dynamics

Duo-Duo Li(李多多) and Song Zhang(张嵩)
Chin. Phys. B, 2022, 31 (**8**): 083103. DOI: 10.1088/1674-1056/ac5607

Plasticity and melting characteristics of metal Al with Ti-cluster under shock loading

Dong-Lin Luan(栾栋林), Ya-Bin Wang(王亚斌), Guo-Meng Li(李果蒙), Lei Yuan(袁磊), and Jun Chen(陈军)
Chin. Phys. B, 2021, 30 (**7**): 073103. DOI: 10.1088/1674-1056/abe1a0

State-to-state dynamics of reactions H+DH'(v = 0,j = 0) → HH'(v',j')+D/HD(v',j')+H' with time-dependent quantum wave packet method

Juan Zhao(赵娟), Da-Guang Yue(岳大光), Lu-Lu Zhang(张路路), Shang Gao(高尚), Zhong-Bo Liu(刘中波), and Qing-Tian Meng(孟庆田)
Chin. Phys. B, 2021, 30 (**7**): 073102. DOI: 10.1088/1674-1056/abf559

Size effect of He clusters on the interactions with self-interstitial tungsten atoms at different temperatures

Jinlong Wang(王金龙), Wenqiang Dang(党文强), Daping Liu(刘大平), Zhichao Guo(郭志超)
Chin. Phys. B, 2020, 29 (**9**): 093101. DOI: 10.1088/1674-1056/ab9619

SPECIAL TOPIC — Ultrafast physics in atomic, molecular and optical systems

Theoretical study of the light-induced conical intersection in the photodissociation of molecule OH

Jinqian Liu(刘金倩)[1,2], Jialong Li(李嘉隆)[1,2], Dongdong Zhang(张栋栋)[1,2,†], and Dajun Ding(丁大军)[1,2,‡]

[1] *Institute of Atomic and Molecular Physics, Jilin University, Changchun* 130012, *China*

[2] *Jilin Key Laboratory of Atomic and Molecular Spectroscopy, Jilin University, Changchun* 130012, *China*

(Received 1 March 2025; revised manuscript received 23 April 2025; accepted manuscript online 23 May 2025)

Light-induced conical intersections (LICIs) present a distinctive mechanism for nonadiabatic coupling, thereby facilitating ultrafast chemical reactions, including the indirect photodissociation of diatomic molecules. In contrast to static conical intersections, LICIs are dynamically tunable, providing a pathway for precise control of molecular dissociation. In this study, we employ the time-dependent quantum wave packet method to investigate the dissociation dynamics of the OH molecule, focusing on its ground state $X^2\Pi$ and repulsive state $1^2\Sigma^-$. By varying laser field parameters (intensity, full width at half maximum (FWHM), and wavelength), we elucidate how nonadiabatic coupling governs selective dissociation channel control. Our findings reveal that the choice of initial vibrational states and the tailoring of laser conditions significantly influence dissociation pathways, providing theoretical insights into manipulating molecular dynamics via LICIs. These results provide a foundation for future experimental studies and the development of advanced molecular control techniques.

Keywords: light-induced conical intersection, indirect photodissociation, time-dependent quantum wave packet method

PACS: 31.15.xv

DOI: 10.1088/1674-1056/addcbb **CSTR:** 32038.14.CPB.addcbb

1. Introduction

Conical intersections (CIs) are pivotal in molecular quantum dynamics, enabling efficient nonadiabatic transitions between electronic states. These phenomena govern a wide range of processes in chemical reaction dynamics, molecular spectroscopy, biochemistry, biophysics, photochemistry, and photophysics.[1–14] In diatomic molecules, the lack of the complex vibrational and rotational degrees of freedom present in polyatomic systems often results in avoided crossings rather than true CIs. However, introducing an external laser field adds a controllable degree of freedom, allowing the formation of light-induced conical intersections (LICIs).[13,15] LICIs offer distinct advantages over intrinsic conical intersections due to their tunable parameters, including laser intensity, frequency, and polarization. These features enable precise control of nonadiabatic coupling, thereby influencing molecular dissociation dynamics and reaction pathways. Recent theoretical and experimental advances have demonstrated the potential of LICIs in guiding chemical reactions, yet a comprehensive understanding of their effects on diatomic molecular dissociation remains incomplete.

The OH molecule serves as an ideal system for investigating LICIs due to its simple electronic structure. In this study, we employ the time-dependent quantum wave packet method to explore the dissociation dynamics of OH, incorporating both vibrational and rotational degrees of freedom. By systematically varying laser field parameters — including intensity, pulse duration, and wavelength — we aim to achieve selective control over dissociation channels. This approach provides theoretical insights into the interplay between LICIs and nonadiabatic coupling, contributing to the broader goal of developing tunable molecular control mechanisms and offering a more comprehensive framework for understanding molecular dissociation in the presence of LICIs.

2. Theoretical method

In this paper, we focus on the OH molecule, a two-electron system, consisting of the ground state $X^2\Pi$ and the repulsive state $1^2\Sigma^-$.[16] The potential energy curves are shown in Fig. 1.

The interaction of these states with a linearly polarized laser field is modeled using the time-dependent Schrödinger equation (TDSE) under the Born–Oppenheimer approximation. The Hamiltonian governing the system is expressed as

$$\hat{H}(t) = \hat{T} + V_{\text{diab}} + V_{\text{laser}}(t), \tag{1}$$

where $\hat{T}$ represents the nuclear kinetic energy, V_{diab} is the diabatic potential energy matrix, and $V_{\text{laser}}(t)$ describes the inter-

†Corresponding author. E-mail: dongdongzhang@jlu.edu.cn

‡Corresponding author. E-mail: dajund@jlu.edu.cn

© 2025 Chinese Physical Society and IOP Publishing Ltd. All rights, including for text and data mining, AI training, and similar technologies, are reserved.

action with the laser field. The TDSE can be expressed as

$$\mathrm{i}\hbar\frac{\partial}{\partial t}\Psi(R,\theta,t)=\hat{H}(R,\theta,t)\Psi(R,\theta,t), \tag{2}$$

where

$$\Psi(R,\theta,t)=\begin{pmatrix}\psi_{\mathrm{g}}\\ \psi_{\mathrm{e}}\end{pmatrix}, \tag{3}$$

where ψ_{g} and ψ_{e} represent the wave functions of the ground state $X^2\Pi$ and the repulsive state $1^2\Sigma^-$, respectively. The form of the electric field is given by

$$\boldsymbol{E}(t)=\hat{e}_z\varepsilon_0 f(t)\cos(\omega_0 t), \tag{4}$$

where $\hat{e}_z$ is the polarization direction, ε_0 is the maximum field amplitude, ω_0 is the carrier frequency, and $f(t)$ is the carrier envelope function

$$f(t)=\exp\left(-\frac{4\ln 2}{t_{\mathrm{p}}^2}t^2\right), \tag{5}$$

where t_{p} denotes the full width at half maximum (FWHM) of the pulse.

In the electric-dipole approximation, the molecule–laser interaction Hamiltonian $\hat{H}(R,\theta,t)$ is expressed as

$$\hat{H}(R,\theta,t)=\begin{pmatrix}-\frac{\hbar^2}{2\mu}\frac{\partial^2}{\partial R^2}+\frac{\hat{J}^2}{2\mu R^2} & 0\\ 0 & -\frac{\hbar^2}{2\mu}\frac{\partial^2}{\partial R^2}+\frac{\hat{J}^2}{2\mu R^2}\end{pmatrix}+\begin{pmatrix}V_{\mathrm{g}}(R) & -d(R)\cos\theta\varepsilon_0 f(t)\cos(\omega_0 t)\\ -d(R)\cos\theta\varepsilon_0 f(t)\cos(\omega_0 t) & V_{\mathrm{e}}(R)\end{pmatrix}, \tag{6}$$

where $d(R)$ is the transition dipole moment between the two diabatic electronic states, μ is the reduced mass, $\hat{J}^2$ is the angular momentum operator of nuclear rotation, $\hat{e}_z$ is the laser polarization direction, and θ is the angle between the polarization direction and the molecular axis.

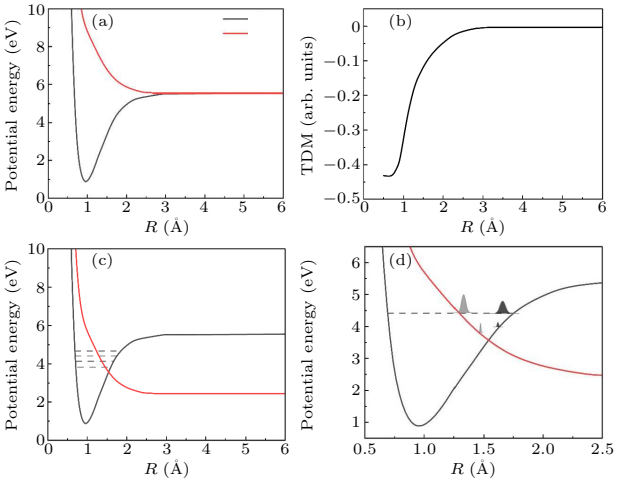


Fig. 1. Schematic illustration of the photodissociation reaction of the OH molecule.[17] (a) Field-free potential energy surfaces of the OH molecule.[17] (b) Transition dipole moment between the ground state $X^2\Pi$ and the repulsive state $1^2\Sigma^-$. (c) Schematic of the light-induced conical intersection (LICI), where the dotted lines indicate vibrational levels $v=8,9,10,11$. (d) Two approaches for wave packet dissociation.

By diagonalizing the diabatic potential energy matrix in Eq. (6), two time-dependent light-induced potentials (LIPs), $V_{\mathrm{g}}^{\mathrm{LIP}}$ and $V_{\mathrm{e}}^{\mathrm{LIP}}$, can be expressed as

$$V_{\mathrm{g}}^{\mathrm{LIP}}(R,\theta,t)=\frac{1}{2}\left(V_{\mathrm{e}}(R)-\hbar\omega_0+V_{\mathrm{g}}(R)-\sqrt{\Delta^2+4C^2(t)}\right), \tag{7}$$

$$V_{\mathrm{e}}^{\mathrm{LIP}}(R,\theta,t)=\frac{1}{2}\left(V_{\mathrm{e}}(R)-\hbar\omega_0+V_{\mathrm{g}}(R)+\sqrt{\Delta^2+4C^2(t)}\right), \tag{8}$$

where the detuning is defined as $\Delta=V_{\mathrm{e}}(R)-\hbar\omega_0-V_{\mathrm{g}}(R)$, and the diabatic coupling $C(t)$ is given by $C(t)=-\frac{1}{2}\cos\theta\,\varepsilon_0 f(t)d(R)$. A light-induced conical intersection is formed only when both $\Delta=0$ and $C(t)=0$, i.e., when $\cos\theta=0$ ($\theta=\pi/2$) and $V_{\mathrm{g}}(R)=V_{\mathrm{e}}(R)-\hbar\omega_0$.

The initial molecular wave function is a direct product of the initial vibrational and rotational wave functions

$$\Psi_M(R,\theta,t_0)=\chi_{v,J}(R)P_J^M(\cos\theta), \tag{9}$$

where $P_J^M(\cos\theta)$ are the eigenfunctions of the rotational angular momentum operator

$$\left[\frac{1}{\sin\theta}\frac{\partial}{\partial\theta}\left(\sin\theta\frac{\partial}{\partial\theta}\right)+\frac{M^2}{\sin^2\theta}-\hbar^2J(J+1)\right]P_J^M(\cos\theta)=0, \tag{10}$$

and $\chi_{v,J}(R)$ is the radial wave function, whose eigenequation can be solved using the Fourier grid Hamiltonian method

$$\left[-\frac{\hbar^2}{2m}\frac{\partial^2}{\partial R^2}+\frac{\hbar^2J(J+1)}{2mR^2}+V_{\mathrm{g}}(R)-\varepsilon_{v,J}\right]\chi_{v,J}(R)=0, \tag{11}$$

where $\varepsilon_{v,J}$ is the eigenvalue of the radial wave function.

We solve the TDSE using the split-operator method. The probability of observing fragments is given by

$$P(E,\theta,t)\equiv|\langle E,p|\Psi_{\mathrm{e}}(\theta,t)\rangle|^2,\propto\left|\sum_{vJ}c_{vJ}V_{vJME}\frac{\mathrm{e}^{-\frac{(E_v+E_{JM})t}{\hbar}}-1}{\frac{E_v+E_{JM}-E}{\hbar}}P_J^M(\cos\theta)\right|^2, \tag{12}$$

where $V_{vJME}=\langle E,p|V_{\mathrm{c}}|E_vE_{JM}\rangle$ is the coupling matrix element between the two resonance states, and the total fragmentation energy is $E=\frac{p^2}{2\mu}+D_0$, with D_0 being the dissociation energy of O+H.

3. Results and discussion

In this study, we employ the time-dependent quantum wave packet method to investigate the evolution of the excited-state wave packet, focusing on the reaction intermediate OH^*. By solving the TDSE, we obtain the propagation dynamics of two wave packets on the nonadiabatic potential energy surfaces. The linearly polarized laser field, $\boldsymbol{E}(t)$, is centered at $t = 0$. We analyze the dissociation dynamics of the OH molecule by varying laser parameters, including intensity, FWHM, and wavelength.

The initial nuclear wave function is assumed to reside in a single eigenstate of the ground state with an initial rotational quantum number $J = 0$. The initial vibrational state is chosen such that its energy exceeds that of the LICI point ($E_v > E_{\mathrm{LICI}}$). The nuclear coordinate range is set from 0.5 Å to 105.5 Å, with the absorbing potential positioned at $R =$ 100.5 Å. Absorbing boundary conditions are implemented to prevent unphysical reflections at the grid edges, facilitating accurate simulation of the dissociation process. As different laser wavelengths correspond to varying photon energies, the required number of grid points varies accordingly. In our simulations, we uniformly employ 4096 grid points to ensure adequate spatial resolution across all scenarios. This approach aligns with established practices in time-dependent quantum wave packet dynamics, where sufficient grid density is crucial for capturing the nuances of wave packet evolution. Further computational details and methodological specifics can be found in Refs. [18–21].

We focus on the dissociation dynamics of the OH molecule under a 400 nm laser field, considering vibrational states above the LICI, specifically levels $v = 8$, 9, 10, and 11, as depicted in Fig. 1(c). Our analysis reveals that the initial nuclear wave packet of OH transitions rapidly to the excited state near the peak of the laser pulse and subsequently dissociates within approximately 50 fs, as illustrated in Fig. 2. This rapid dissociation indicates a change in the number of available channels after dissociation, a hallmark of indirect photodissociation processes. Understanding these dynamics provides deeper insights into the dissociation mechanisms of the OH molecule and offers potential strategies for manipulating its dissociation pathways.

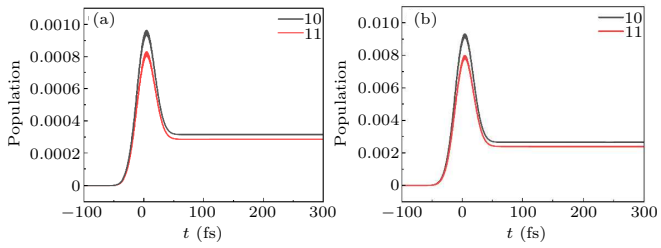


Fig. 2. Time evolution of the excited-state population. Laser intensities are (a) 10^{13} W/cm^2 and (b) 10^{14} W/cm^2. The black and red lines represent initial vibrational states $v = 10$ and $v = 11$, respectively.

Our study indicates that the selection of the initial vibrational state significantly influences the dissociation dynamics of OH molecules. As depicted in Fig. 3, the angular distributions of dissociated O and H fragments from initial vibrational states $v = 8$ and 9 show a single dissociation channel at different observation times, with a narrowed energy distribution. Conversely, for $v = 10$ and 11, two dissociation channels are observed at $t = 100$ fs. This bifurcation results from the participation of two electronic states, naturally leading to two dissociation pathways, consistent with our expectations.

Under a laser field characterized by a 400 nm wavelength, an intensity of 1×10^{13} W/cm^2, and a full width at half maximum of 50 fs, our findings indicate that indirect photodissociation does not occur for initial vibrational states $v = 8$ and 9. In contrast, for $v = 10$ and 11, the OH molecule undergoes indirect photodissociation via the intermediate OH^*. These observations highlight the crucial role of the initial vibrational state in determining the dissociation pathway. By modulating laser field parameters, we can probe the intermediate OH^*, thus improving our understanding of its dissociation dynamics. This approach facilitates the manipulation of dissociation processes through strategic selection of initial vibrational states. In subsequent investigations, we will compare the dissociation phenomena for $v = 10$ and 11 to elucidate the underlying physical mechanisms governing these processes.

We further investigate the influence of varying laser intensities on the dissociation dynamics of OH molecules. At laser intensities below 10^{13} W/cm^2, channel selection is absent, and the primary dissociation channel consistently has higher energy than the secondary one. However, as illustrated in Figs. 4(a)–4(c), increasing the laser intensity results in a notable shift: the energy of the primary dissociation channel transitions from higher energy at 4×10^{13} W/cm^2 to lower energy at 10^{14} W/cm^2, thereby achieving channel selection in the O + H dissociation process. This energy relationship follows the expression $\sqrt{2\mu(\varepsilon + \hbar\omega - D_0)}$, where ε denotes the energy of the initial vibrational state, and D_0 is the dissociation energy of the O–H bond.

These observations align with previous studies on molecular dissociation under intense laser fields, which have demonstrated that increasing laser intensity can significantly alter dissociation pathways and fragment energy distributions. For instance, research on the dissociation dynamics of hydrogen molecular ions has shown that varying laser intensity modulates the kinetic energy spectra of dissociating protons, influencing channel selection and energy distribution.

Our analysis reveals that the emergence of two distinct peaks indicates simultaneous excitation of quasi-bound states situated above and below the resonance state. The higher-energy peak corresponds to the product of $V_{\mathrm{g}}^{\mathrm{LIP}}$, facilitating the transition to the upper quasi-bound state, whereas the lower-energy peak corresponds to $V_{\mathrm{e}}^{\mathrm{LIP}}$, leading to the lower quasi-bound state. This observation suggests that,

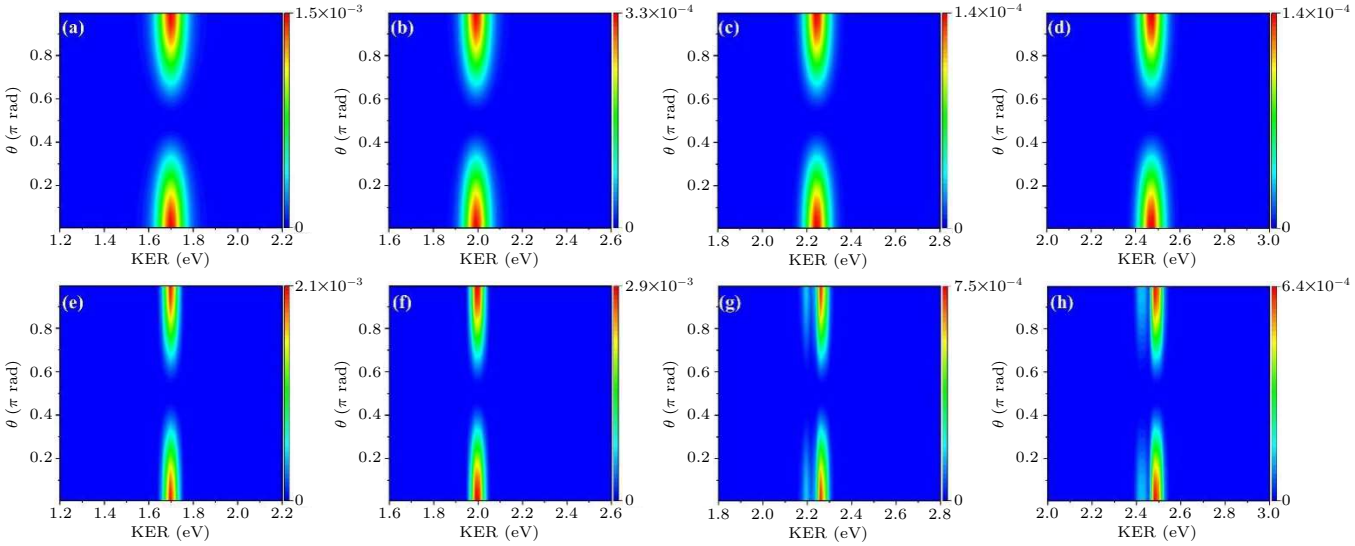


Fig. 3. Probability distributions of the kinetic energy released for O + H at different vibrational states. The top and bottom rows correspond to observations at $t = 20$ fs and $t = 100$ fs, respectively. The initial vibrational states from left to right are $v = 8, 9, 10$, and 11. The laser center wavelength is $\lambda = 400$ nm, $I = 10^{13}$ W/cm^2, and FWHM = 50 fs.

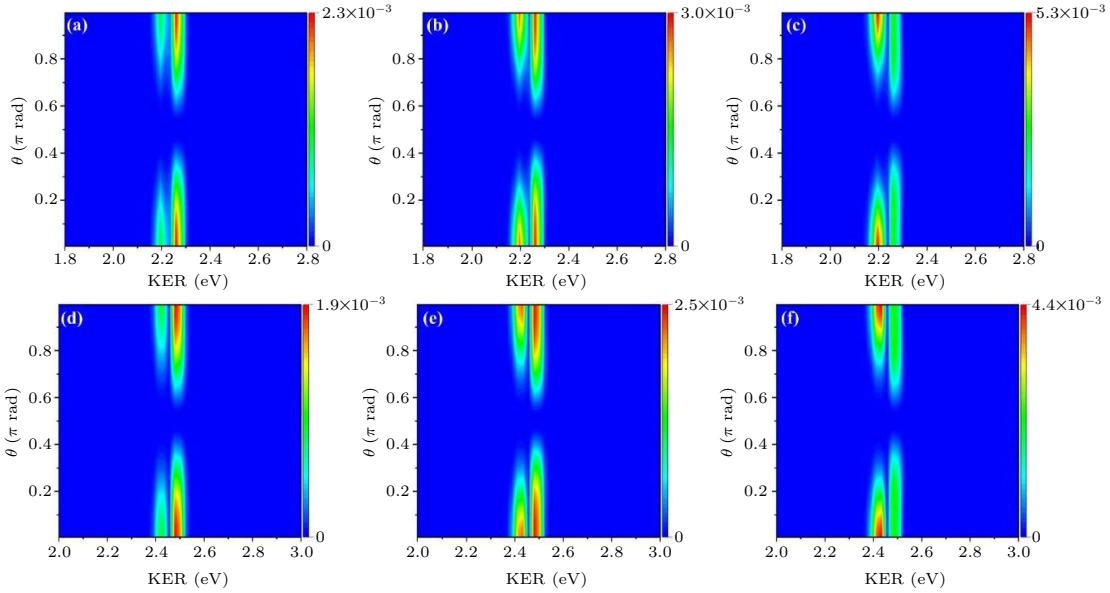


Fig. 4. Probability distributions of the kinetic energy released for O + H at different laser intensities. The top and bottom rows correspond to observations at $v = 10$ and $v = 11$, respectively. The laser intensities from left to right are 4×10^{13} W/cm^2, 7×10^{13} W/cm^2, and 10^{14} W/cm^2, with $\lambda = 400$ nm, FWHM = 50 fs, and $t = 100$ fs.

with increasing laser intensity, OH molecules dissociate more readily along the repulsive state, a phenomenon directly linked to enhanced nonadiabatic coupling between the two states. The observed shift in the energy of the primary dissociation channel provides compelling evidence for channel selection mechanisms. A similar trend is observed for $v = 11$, as shown in Figs. 4(d)–4(f). Notably, compared to $v = 10$, the dissociation fragments (O + H) exhibit higher energies, attributable to the elevated energy of the initial vibrational state, as illustrated in Fig. 1(c). Additionally, the dissociation probability for each channel is slightly lower for $v = 11$, consistent with Fig. 2, which shows that the excited-state population for $v = 10$ consistently exceeds that for $v = 11$ at laser intensities of 10^{13} W/cm^2 and 10^{14} W/cm^2.

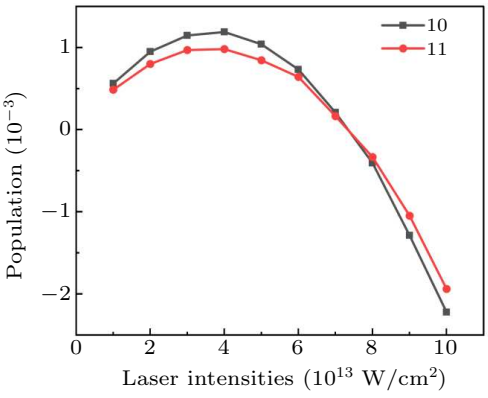


Fig. 5. Difference in the O + H dissociation channel populations at different laser intensities (right channel minus left channel). The black and red lines correspond to observations at $v = 10$ and $v = 11$, respectively. The laser parameters are $\lambda = 400$ nm, FWHM = 50 fs, and $t = 100$ fs.

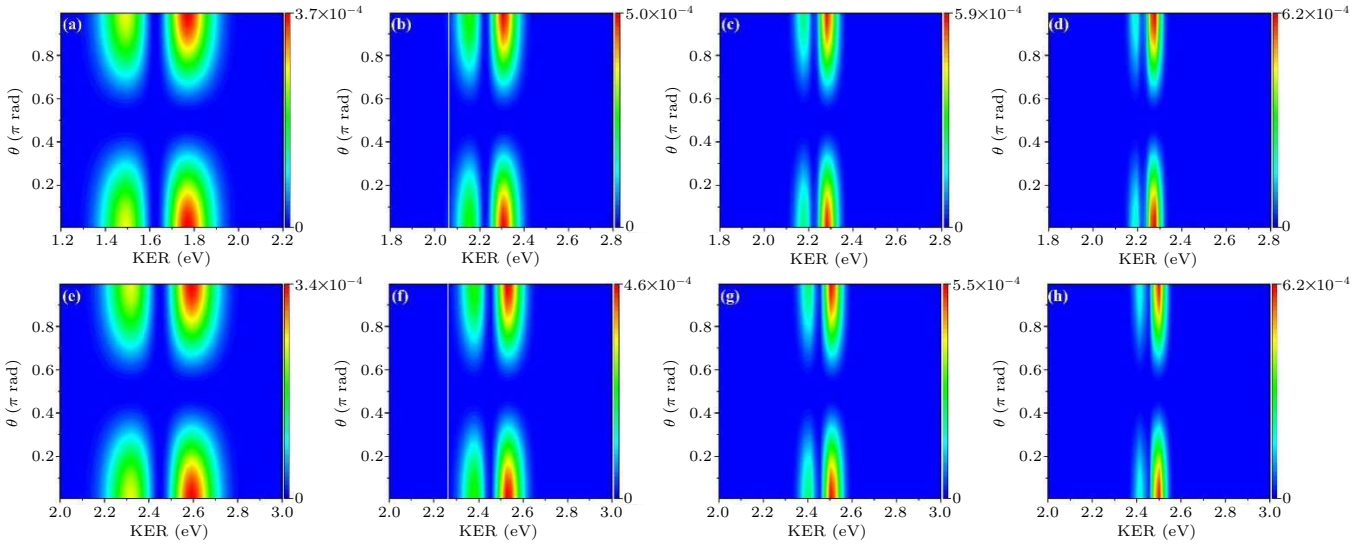


Fig. 6. Probability distributions of the kinetic energy released for O + H at different FWHMs. The top and bottom rows correspond to observations at $v = 10$ and $v = 11$, respectively. The FWHMs from left to right are 10 fs, 20 fs, 30 fs, and 40 fs, with $\lambda = 400$ nm, $I = 10^{13}$ W/cm^2, and $t = 100$ fs.

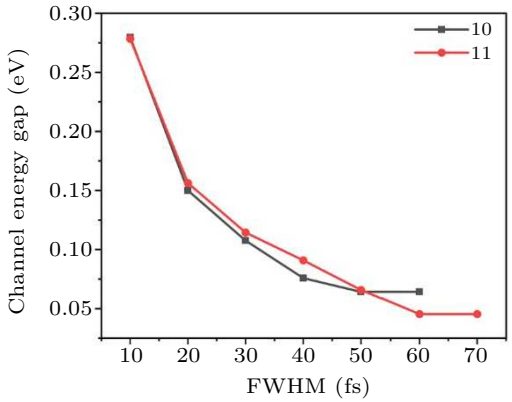


Fig. 7. Variation of the energy gap between the two dissociation channels of the dissociated O + H fragment as a function of FWHM. The laser intensity is 10^{13} W/cm^2.

Figure 5 provides a visual representation of the competition between dissociation channels by showing the differential probability between the high-energy and low-energy channels at varying laser intensities. As the intensity increases, the probability difference initially rises, then decreases, and eventually becomes negative. This behavior results from the nonadiabatic coupling between the two electronic states: at low intensities, the coupling is weak, favoring the high-energy channel. Above a certain intensity threshold, enhanced coupling leads to a competitive selection, with the low-energy channel becoming dominant. Furthermore, the population difference for the initial vibrational state $v = 10$ consistently exceeds that for $v = 11$, likely related to the excited-state populations shown in Fig. 2.

These findings underscore the crucial role of laser intensity and initial vibrational states in modulating nonadiabatic coupling and dissociation dynamics, offering valuable insights for controlled molecular dissociation.

To elucidate the influence of laser pulse duration on the energy separation between dissociation channels, we conducted a series of calculations examining the dissociation dynamics of OH molecules at varying FWHM for initial vibrational states $v = 10$ or 11. Our findings, shown in Fig. 6, indicate that for both vibrational states, narrower FWHM values (e.g., 10 fs) produce broader energy distributions for the two dissociation channels compared to wider FWHM values (e.g., 40 fs). This broadening, however, is accompanied by a decrease in overall dissociation probability. As shown in Fig. 7, the energy gap between the two channels decreases with increasing FWHM, most notably when the FWHM increases from 10 fs to 20 fs, after which the reduction becomes more gradual. Notably, the channel energy gap for $v = 11$ consistently exceeds that of $v = 10$. For $v = 10$, dual-channel dissociation vanishes when the FWHM exceeds 60 fs, while for $v = 11$, the threshold occurs at 70 fs. We posit that narrower laser pulses concentrate energy more effectively, preferentially exciting specific vibrational states and influencing the energy disparity between dissociation channels.

This observation aligns with previous studies showing that laser pulse duration significantly affects molecular dissociation dynamics. For example, research on the dissociation of O_2 molecules under intense laser fields has shown that shorter pulse durations lead to broader energy distributions of dissociation fragments. These results indicate that selecting an appropriate laser FWHM is crucial to achieve dual-channel indirect dissociation while maintaining suitable energy separation and dissociation probabilities.

We also explored the influence of varying wavelengths on the OH dissociation dynamics. For both initial vibrational states ($v = 10$ and $v = 11$), a consistent trend is observed: at 401 nm, the high-energy dissociation channel dominates. As the wavelength increases to 403 nm, the probability of the high-energy channel decreases, while the low-energy channel

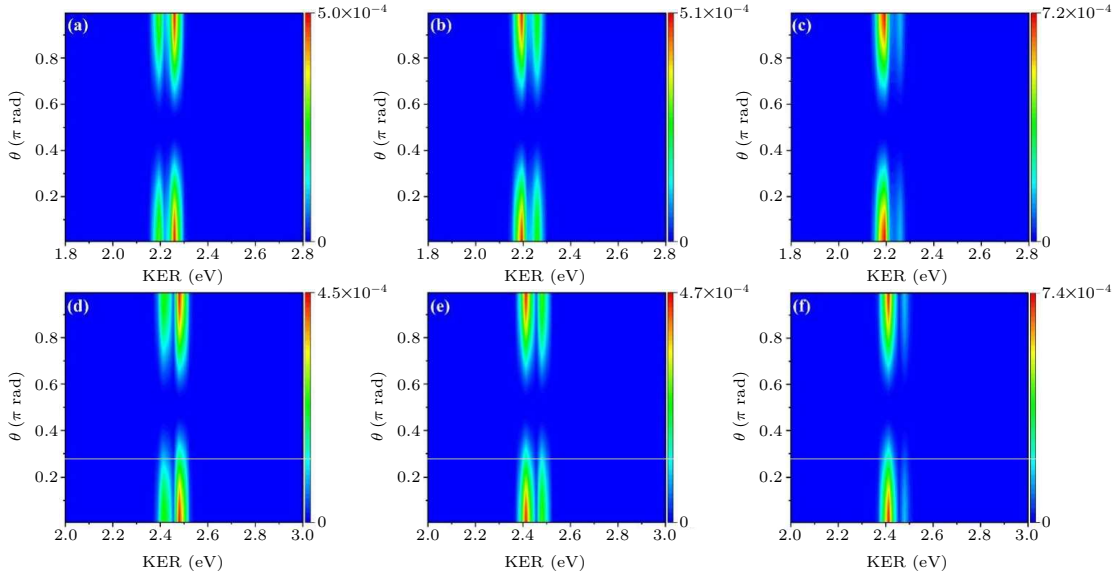


Fig. 8. Probability distributions of the kinetic energy released for O + H at different wavelengths. The top and bottom rows correspond to observations at $v = 10$ and $v = 11$, respectively. The wavelengths from left to right are 401 nm, 402 nm, and 403 nm, with FWHM = 50 fs, $I = 10^{13}$ W/cm^2, and $t = 100$ fs.

becomes dominant. This indicates that indirect dissociation occurs within a specific wavelength range, with the choice of wavelength significantly affecting the dominant dissociation pathway. Since the LICI arises from the interaction of the repulsive state absorbing a photon and intersecting with the ground state, we hypothesize that nonadiabatic coupling is enhanced as the system approaches the conical intersection. As a result, the molecule preferentially dissociates along the low-energy channel corresponding to the repulsive state V_e^{LIP}, in agreement with previous observations regarding the effect of diabatic coupling intensity induced by varying laser intensity. A similar trend is observed for different laser intensities, with the excited-state population of $v = 11$ consistently lower than that of $v = 10$ at 10^{13} W/cm^2 and 10^{14} W/cm^2.

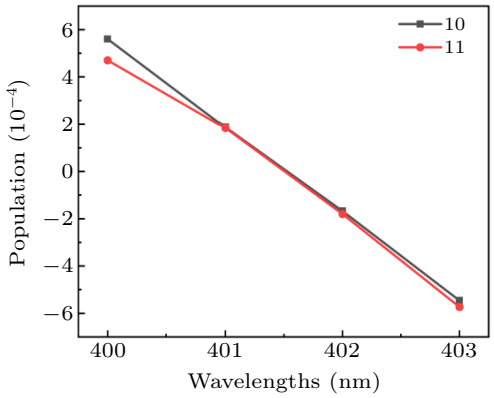


Fig. 9. Difference in the O + H dissociation channel populations at different wavelengths (right channel minus left channel). The black and red lines correspond to observations at $v = 10$ and $v = 11$, respectively. The laser parameters are $I = 10^{13}$ W/cm^2, FWHM = 50 fs, and $t = 100$ fs.

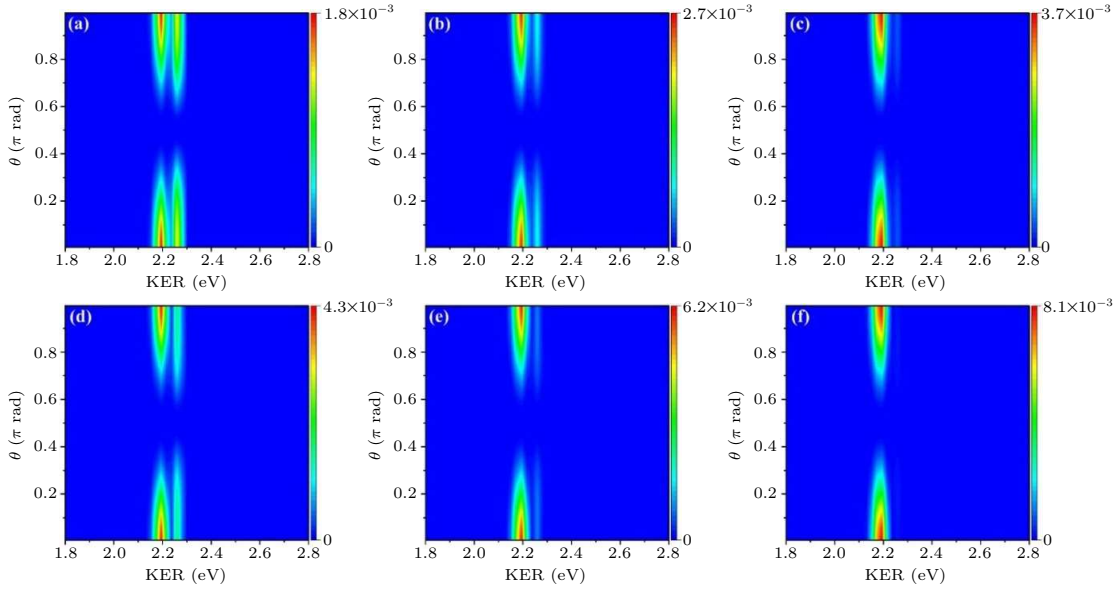


Fig. 10. Changes in the probability distributions of the kinetic energy released for O + H at continuous wavelengths under different laser intensities. The top row corresponds to a laser intensity of 4×10^{13} W/cm^2, and the bottom row corresponds to a laser intensity of 7×10^{13} W/cm^2. The wavelengths from left to right are 401 nm, 402 nm, and 403 nm, with FWHM = 50 fs, $v = 10$, and $t = 100$ fs.

The difference in probabilities between the high-energy (right) and low-energy (left) dissociation channels at successive wavelengths is shown in Fig. 9. As the wavelength increases, the probability difference gradually decreases. This occurs because the initial vibrational state approaches the light-induced conical intersection, enhancing nonadiabatic coupling and promoting selective competition between the dissociation channels. Consequently, the low-energy channel becomes the dominant pathway. Additionally, Fig. 9 shows a trend similar to Fig. 5, with $v = 10$ consistently exhibiting slightly higher dissociation probability than $v = 11$.

To further illustrate the influence of nonadiabatic coupling induced by varying laser intensities and wavelengths (i.e., the position of the LICI), we analyzed cases involving both high laser intensity and long wavelength. As seen in Fig. 8, compared to the high-intensity cases shown in Figs. 4(a) and 4(b), the low-energy dissociation channel becomes more pronounced as the wavelength increases, as shown in Figs. 10(a)–10(f), indicating an increased tendency for dissociation along the excited state.

Furthermore, comparison of Fig. 8(a) with Figs. 10(a) and 10(d) reveals that higher laser intensity further enhances dissociation along the excited state. Overall, these results indicate that simultaneous high laser intensity and long wavelength conditions favor dissociation along the excited state.

4. Conclusion

We investigated the indirect photodissociation dynamics of OH molecules in the presence of LICIs. By systematically varying the parameters of the laser field, we demonstrated selective control of dissociation channels, emphasizing the tunability of LICIs. This study establishes a robust theoretical framework for manipulating molecular dynamics and offers insights that can be extended to more complex molecular systems. While this study focuses on the OH molecule, the principles can be applied to polyatomic systems, where multiple conical intersections and higher-dimensional potential energy surfaces must be considered.

Experimental validation could employ time-resolved spectroscopy with femtosecond laser pulses to monitor population transfer between ground and excited states, while probing LICI formation by varying laser intensity, pulse duration, and wavelength. Future work will focus on rotational-state-selected molecules interacting with femtosecond lasers, using velocity-map imaging to study LICIs in diatomic molecules.

Acknowledgments

We thank Prof. Chuancun Shu for sharing his code with us. This project was supported by the National Natural Science Foundation of China (Grant Nos. 12134005 and 12334011) and the Major Research Plan of the National Natural Science Foundation of China (Grant No. 92461301).

References

[1] Truhlar G D and Mead A C 2003 *Phys. Rev. A* **68** 032501
[2] Baer M 2002 *Phys. Rep.* **358** 75
[3] Worth G A and Cederbaum L S 2004 *Annu. Rev. Phys. Chem.* **55** 127
[4] Matsika S 2007 *Rev. Comput. Chem.* **23** 83
[5] Halasz G J, Vibok A, Sindelka M, Moiseyev N and Cederbaum L S 2011 *J. Phys. B* **44** 175102
[6] Halasz G J, Sindelka M, Moiseyev N, Cederbaum L S and Vibok A 2012 *J. Phys. Chem. A* **116** 2636
[7] Halasz G J, Vibok A, Sindelka M and Cederbaum L S 2012 *Chem. Phys.* **399** 146
[8] Halasz G J, Vibok A, Moiseyev N and Cederbaum L S 2012 *J. Phys. B* **45** 135101
[9] Halasz G J, Vibok A, Meyer H D and Cederbaum L S 2013 *J. Phys. Chem. A* **117** 8528
[10] Halasz G J, Vibok A, Moiseyev N and Cederbaum L S 2013 *Phys. Rev. A* **88** 043413
[11] Halasz G J, Csehi A, Vibok A and Cederbaum L S 2014 *J. Phys. Chem. A* **118** 11908
[12] Halasz G J, Csehi A, Vibok A and Cederbaum L S 2015 *J. Phys. Chem. Lett.* **6** 348
[13] Natan A, Ware M R, Prabhudesai V S, Lev U, Bruner B D, Heber O and Bucksbaum P H 2016 *Phys. Rev. Lett.* **116** 143004
[14] Csehi A, Halász J G, Cederbaum L S and András A 2017 *Phys. Chem. Chem. Phys.* **19** 19656
[15] Csehi A, Halász G J and Vibók Á 2018 *Chem. Phys.* **509** 91
[16] Qin X and Zhang D S 2014 *J. Korean Phys. Soc.* **65** 2017
[17] Li Y and Zhang P 2011 *J. Theor. Comput. Chem.* **10** 747
[18] Shu C C and Henriksen N E 2011 *J. Chem. Phys.* **134** 164308
[19] Shu C C, Yu J, Yuan K J, Hu W H, Yang J and Cong S L 2009 *Phys. Rev. A* **79** 023418
[20] Shu C C, Yuan K J, Dong D, Petersen I R and Bandrauk A D 2017 *J. Phys. Chem. Lett.* **8** 1
[21] Liu Y, Meng Q J, Sun Z G and Shu C C 2024 *J. Phys. Chem. Lett.* **15** 8393